$R_2Fe_{14}B$-TYPE ISOTROPIC POWDERS FOR BONDED MAGNETS

P. CAMPBELL, D.N. BROWN, Z.M. CHEN, P.C. GUSCHL, D.J. MILLER AND B.M. MA
Magnequench Inc., 61 Science Park Rd. #01-17, Singapore Science Park III, Singapore 117525
Corresponding author e-mail:pcampbel@mqii.com

Abstract

Recent improvements to commercially available rapidly solidified powders for isotropic bonded magnet applications have been reviewed. Powders with high B_r alone are not always sufficient to guarantee for high $(BH)_{max}$ magnets. Powders with reasonably high H_{ci} have been found to be necessary for producing high $(BH)_{max}$ bonded magnets. Such powders are based upon near stoichiometric $Nd_2Fe_{14}B$ and $R_2Fe_{14}B/\alpha$-Fe type nanocomposites. The $R_2Fe_{14}B/\alpha$-Fe type nanocomposite has been found to exhibit better demagnetization curve squareness than equivalent $R_2Fe_{14}B/Fe_3B$ type nanocomposites. A microdispersion coating technique has been successfully developed to enhance the environmental stability of conventional flake powders. This coating reduces flux aging loss by up to 50% depending upon the powder grade. Also, microdispersion coating improves the corrosion and oxidation resistance of magnetic powder as evidenced by a reduction in weight gain during 85°C-85% relative humidity trials. Spherical NdFeB-based powder prepared by atomization exhibits superior polymer melt processibility for injection molding compared to conventional melt spun flake powder. However, if melt spun flake is milled to an appropriate particle aspect ratio more close to cubic, then this powder will exhibit similar processing benefits together with the superior magnetic properties of a near stoichiometric composition.

Introduction

Isotropic bonded magnets using melt-spun $R_2Fe_{14}B$-type powder compositions continue to enable major new applications in motors and sensors for the media storage, consumer electronics, automotive, office automation and appliance markets. The magnetic and thermal properties of such powders continue to evolve, while the net-shape formability and improving cost advantages of these magnets give them key advantages over anisotropic alternatives for many major applications. The technical drivers for the use of an $R_2Fe_{14}B$ powder include various combinations of high B_r, high (or low) H_{ci}, high $(BH)_{max}$, good loop squareness, low flux aging loss, good thermal and corrosion stabilities, but the ultimate magnetic performance of the bonded magnet also depends on factors such as the type of polymer binder, volume fraction of magnetic powder, and processibility.

The most recent isotropic melt-spun $R_2Fe_{14}B$ powders introduced by Magnequench have focused on optimizing selected magnetic properties for bonded magnets that are facing increasingly demanding operating conditions: disk drives and various electronic devices are demanding higher B_r materials, sometimes coupled with easier magnetization; automotive and other high temperature applications are demanding lower flux aging losses; and harsher environments require better corrosion resistance. Significant improvements in powder properties include (i) a $R_2Fe_{14}B/\alpha$-Fe type nano-structured powder with B_r of nearly 1T, (ii) a melt spun powder with low flux aging loss suitable for high temperature applications, (iii) a microdispersion coating for powders to enable conventional isotropic $R_2Fe_{14}B$ powders to operate under even more severe environments, (iv) atomized $R_2Fe_{14}B$-type powder of spherical morphology which provides excellent corrosion resistance and also modifies the rheological behavior of the polymer melt during injection molding, and (v) smaller particle sizes of atomized and milled melt-spun $R_2Fe_{14}B$-type powders which enables the production of magnets with highly defined magnetization patterns.

1. High B_r nanocomposite powder

Previously, the highest B_r achieved from melt-spun single-phase $R_2TM_{14}B$ powder was around 900mT (e.g. Magnequench grade MQP™-B). A higher B_r with a modest H_{ci} can be achieved by introducing a magnetically soft phase (typically α-Fe or Fe_3B) to form a nanostructure of finely dispersed α-Fe (or Fe_3B) grains within a matrix of magnetically hard $R_2Fe_{14}B$ [1]. This new type of very fine hard/soft structured material is generally referred to as nanocomposite. In nanocomposite magnets, the soft magnetic phase induces higher B_r by providing a higher magnetic moment, and the hard magnetic phase provides the H_{ci} component via its strong magnetocrystalline anisotropy. It is the magnetic exchange coupling interaction between the nano-sized soft and hard phases that leads to an enhanced B_r (and a higher $(BH)_{max}$), and a smooth second quadrant demagnetization curve along with a moderate H_{ci}. The most important requirement is that the grain sizes of both the hard and soft phases be very small (in the range of 10-30 nm) in order to maximize the inter-grain exchange coupling interaction and to optimize the remanence enhancement.

A new type of $R_2TM_{14}B$/α-Fe nanocomposite powder is now commercially produced by Magnequench as grade MQP™-16-7. This powder has magnetic properties of B_r= 980mT, H_{ci} = 557kA/m and $(BH)_{max}$ = 127kJ/m^3. Figure 1 shows the second quadrant demagnetization curve and thermomagnetic analysis scan of the new powder respectively. It is clear that this MQP™-16-7 powder consists of two magnetic phases, the magnetically hard $R_2Fe_{14}B$ and magnetically soft α-Fe, with a typical grain size in the range of 20-30nm.

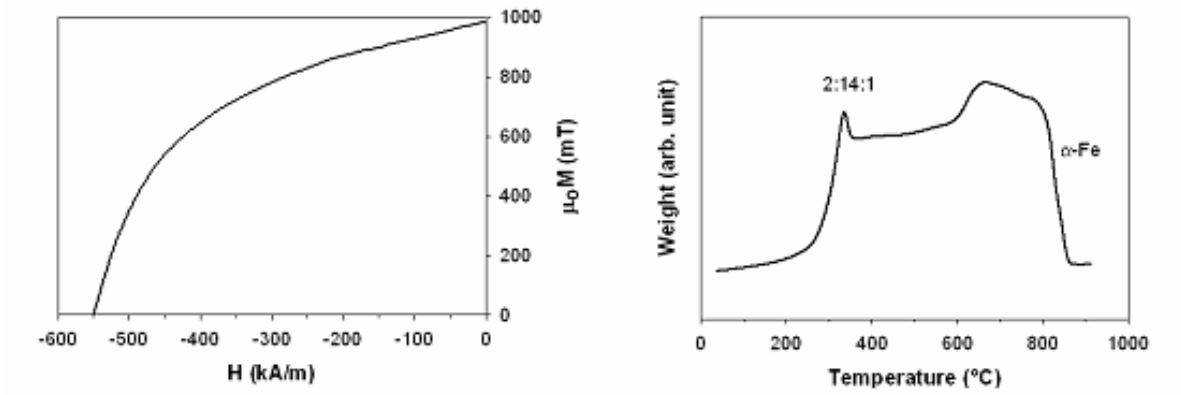

Figure 1: Second quadrant demagnetization curve and thermomagnetic analysis scan of MQP™-16-7 powder.

It should be noted that the $R_2Fe_{14}B$/α-Fe type nanocomposite is more desirable than the $R_2Fe_{14}B/Fe_3B$ type for bonded magnets applications. The $R_2Fe_{14}B$/α-Fe nanocomposite exhibits higher magnetic properties and a more uniform microstructure when compared to equivalent $R_2Fe_{14}B/Fe_3B$ nanocomposites. Figure 2, for example, compares the typical demagnetization curves of an $R_2Fe_{14}B$/α-Fe powder and an $R_2Fe_{14}B/Fe_3B$ powder. As can be seen, the $R_2Fe_{14}B$/α-Fe powder exhibits a higher B_r and much better demagnetization curve squareness than the $R_2Fe_{14}B/Fe_3B$ powder. A good squareness in the demagnetization curve is very important to magnet applications. A reason for the

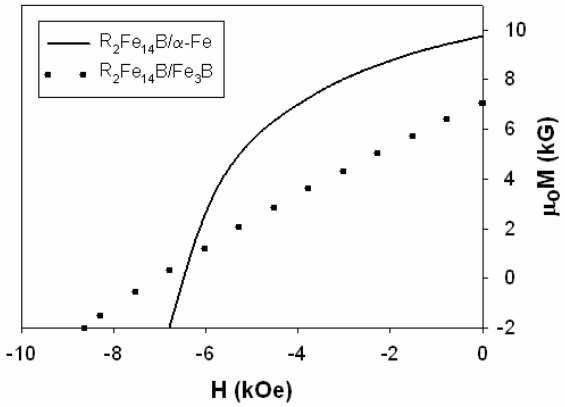

Figure 2: Comparison of the second quadrant demagnetization curves of $R_2Fe_{14}B$/α-Fe and $R_2Fe_{14}B/Fe_3B$ nanocomposites with identical amount of soft magnet phase.

superior squareness may be due to the ability of $R_2Fe_{14}B$ and α-Fe grains to nucleate and grow in a much finer and uniform fashion than in an equivalent $R_2Fe_{14}B/Fe_3B$ microstructure. Such a feature is illustrated in Figure 3.

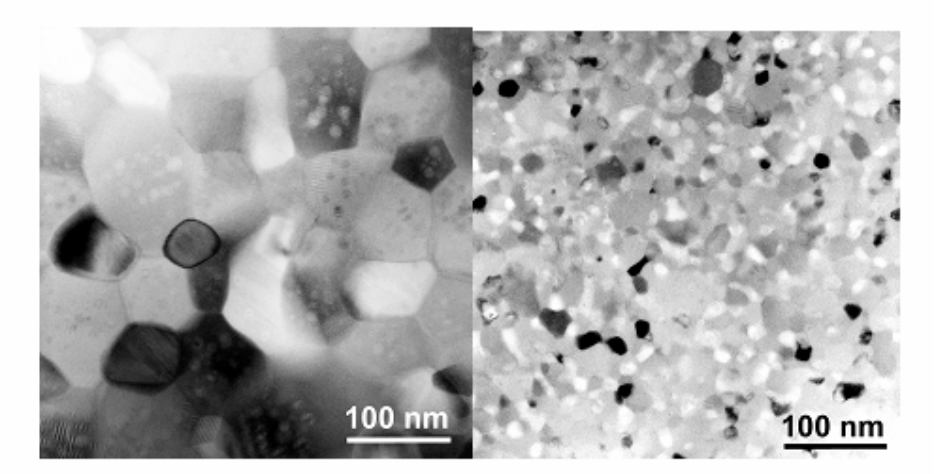

Figure 3: Comparison on the microstructure of $R_2Fe_{14}B/Fe_3B$ (left) and $R_2Fe_{14}B$/α-Fe (right) nanocomposites with identical amount of soft magnetic phase.

Although it is well known that the B_r of nanocomposite increases with the increasing amount of soft magnetic phase, it should also be noted that such benefits are not reflected in the $(BH)_{max}$ of $R_2Fe_{14}B$/α-Fe nanocomposites. Figure 4 illustrates the relationship between B_r, H_{ci} and $(BH)_{max}$ for a range of α-Fe fractions. The nominal compositions of this alloy series vary along the $Pr_2Fe_{14}B$ and α-Fe tie line. As expected, B_r increases and H_{ci} decreases with increasing amounts of α-Fe. Despite the increase in B_r, the $(BH)_{max}$ unexpectedly (since $(BH)_{max} \approx B_r^2$) decreases with the increasing amount of α-Fe. This suggests a high B_r value alone is insufficient to guarantee a high $(BH)_{max}$ value for the nanocomposite. To obtain a nanocomposite of high $(BH)_{max}$, one must balance the B_r, H_{ci} and demagnetization curve squareness. Although alloying elements have been known to refine R-Fe-B nanocomposite microstructures to yield improved overall magnetic performance [2,3,4], the demagnetization curve squareness of nanocomposites is, in general, inferior to near-stoichiometric $R_2Fe_{14}B$ compositions produced by the same production technique.

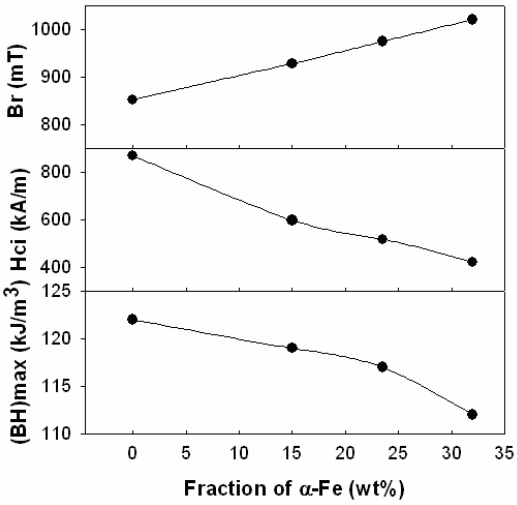

Figure 4: The relationship of B_r, H_{ci} and $(BH)_{max}$ with respect to the amount of α-Fe for an alloy series along the $Pr_2Fe_{14}B$ and α-Fe tie line.

2. High temperature and low flux aging loss powder

A new single-phase $Nd_2Fe_{14}B$-type powder, now commercially produced by Magnequench as grade MQP™-14-12, has been developed for high temperature applications up to 180°C, such as automotive "under the hood" devices. Figure 5 shows the demagnetization curves of MQP™-14-12 at temperatures from 22 to 180°C. The magnetic properties at room temperature are B_r = 840mT, H_{ci} = 955kA/m, and $(BH)_{max}$ = 111kJ/m^3. The B-H line remains straight at temperatures up to 180°C, which is important to ensure irreversible losses are minimized at elevated temperatures. Moreover, as shown in Table 1 and Figure 6, MQP™-14-12 powder exhibits a very low temperature coefficient of

H_{ci} (β) and flux aging loss (δ_{irr}). Temperature coefficients and flux aging loss are two principal quantitative indicators of thermal stability. Flux aging loss defines the amount of magnetic flux lost from a fully magnetized magnet of fixed geometry following exposure to an elevated temperature for a certain amount of time. Such a loss can be divided into two components: spin relaxation and corrosion/oxidation. The former tends to occur when the magnet is initially exposed to the elevated temperature, while the latter usually occurs after the magnet has been exposed to elevated temperature for an extended period of time. Our research has indicated that essential characteristics to achieve low flux aging loss in bonded magnets are that H_{ci} must remain high at elevated temperature, grain size distribution must be fine and uniform, and there should be a minimum amount of soft magnetic and secondary phases.

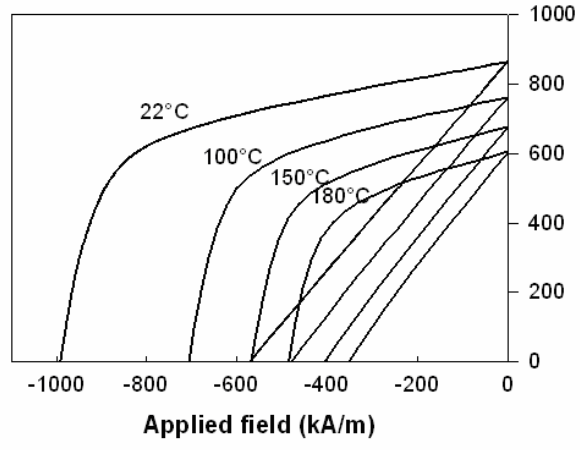

Figure 5: Second quadrant demagnetization curves of MQP™-14-12 measured from 25 to 180°C.

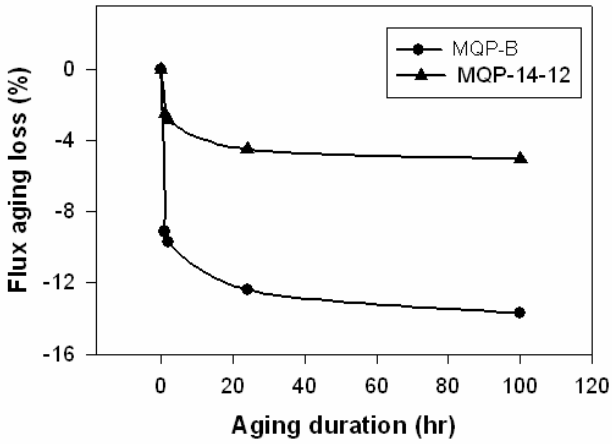

Figure 6: Comparison on the flux aging loss of bonded magnets prepared from MQP™-B and MQP™-14-12, aged at 180°C in dry air.

Table 1: The B_r, H_{ci} and $(BH)_{max}$, α and β of MQP™-14-12 and MQP™-B powders at 22 and 180°C and flux aging loss of bonded magnets with PC=2 (h = 7mm; dia. = 10mm) after aging at 180°C for 100 hours.

Powder type	B_r (mT)		α (%/°C)	H_{ci} (kA/m)		β (%/°C)	BH_{max} (kJ/m^3)		δ_{irr}
	22°C	180°C		22°C	180°C		22°C	180°C	%
MQP™-B	883	675	-0.15	777	358	-0.35	123	56	-13.7
MQP™-14-12	848	616	-0.17	983	494	-0.32	118	58	-5.0

3. Microdispersion coated powder

Despite the foregoing, the required operating temperature of some bonded magnet applications continues to rise, and modifications to alloy composition alone are not sufficient to provide low flux aging loss. One method of further improving the flux aging loss is to apply a coating of an organic material to the melt spun powder. The organic coating deposits itself along the surface of the powder particles, creating a protective barrier between the powder and any potential reactant. Powder prepared via this route is referred to as "microdispersion coated powder" in this work. Certain polymeric materials are ideal for coating in this respect due to their ability to encapsulate large areas of fine, metallic powder.

3.1 Improvement in flux aging loss

Figure 7 shows the flux aging loss of bonded magnets prepared from *microdispersion-coated* MQP-B+™ and MQP™-14-12 with their corresponding controls aged at various temperatures from

80 – 225°C for 100 hours. If a flux aging loss of 5% is deemed an acceptable limit (for example), one can see that the new microdispersion coating allows the magnet operating temperature to increase from 122 to 155°C for magnets prepared from MQP™-B+ and from 146 to 189°C for magnets prepared from MQP™-14-12. Thus, the magnet's maximum operating temperature is raised by more than 30°C using the new formulation for each powder type. It is also interesting to note that the microdispersion-coated MQP™-14-12 powders may be used in applications within the 200 – 220°C range with no more than a 10% loss of flux.

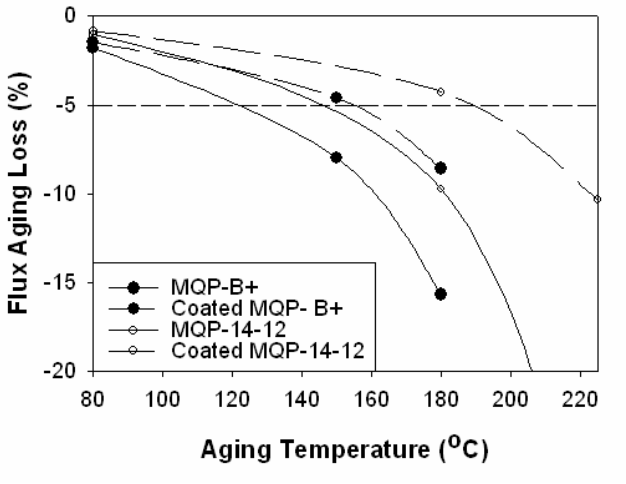

Figure 7: Flux aging loss vs. temperature after 100 hours for magnets using MQP™-B+ and MQP™-14-12 (solid lines) and microdispersion-coated MQP™-B+ and MQP™-14-12 (dashed lines).

The improvement in flux aging loss can be attributed to the fact that the microdispersion coating promotes better coverage to the powder particle surfaces than in the uncoated control. Figure 8 exhibits this quite well for both epoxy liquid coated powders. The dark regions on the powders represent the organic elements of the coating in both micrographs.

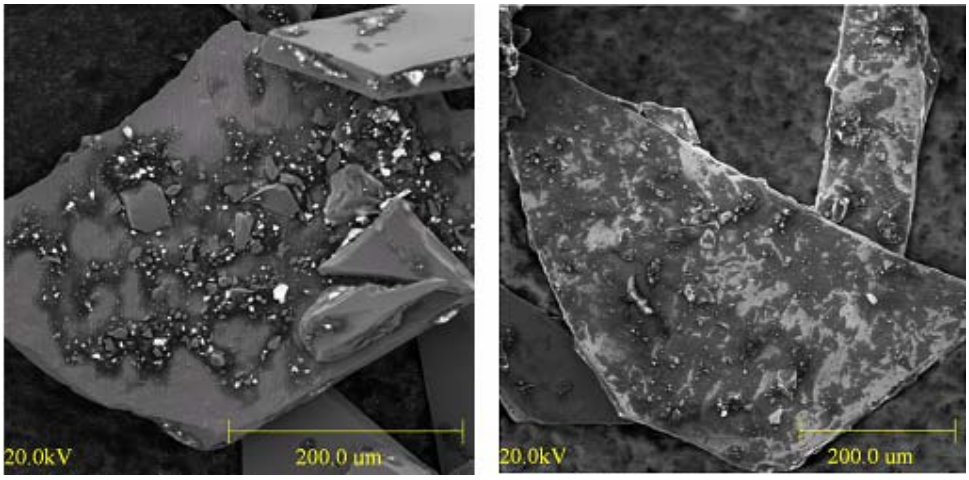

Figure 8: SEM micrographs of control liquid coated powders (left) and microdispersion-coated powders (right).

3.2 Improvement in corrosion resistance

Figure 9 compares the weight gain of bonded magnets prepared from microdispersion coated MQP™-B+ and MQP™-14-12 together with their corresponding controls following exposure to 85°C at 85% relative humidity (RH) over a period of time. A power law relationship can be fitted for the weight change with respect to time under the test conditions. Magnets prepared from the microdispersion coated powders exhibit up to 50% less weight gain than the control samples. A lower weight gain implies an improvement in the corrosion resistance of powders.

3.3 Improvement in physical properties

In addition to the protective capability of the microdispersion coating, improvements of certain physical characteristics were also noted. The porosity of the resulting magnets, which is directly

determined from specific density measurement, was found to increase by approximately 20%. The ejection pressure (the force required to eject the green magnets from compaction) was also found to decrease for the microdispersion coated materials. Both are beneficial to bonded magnet manufacturing and applications.

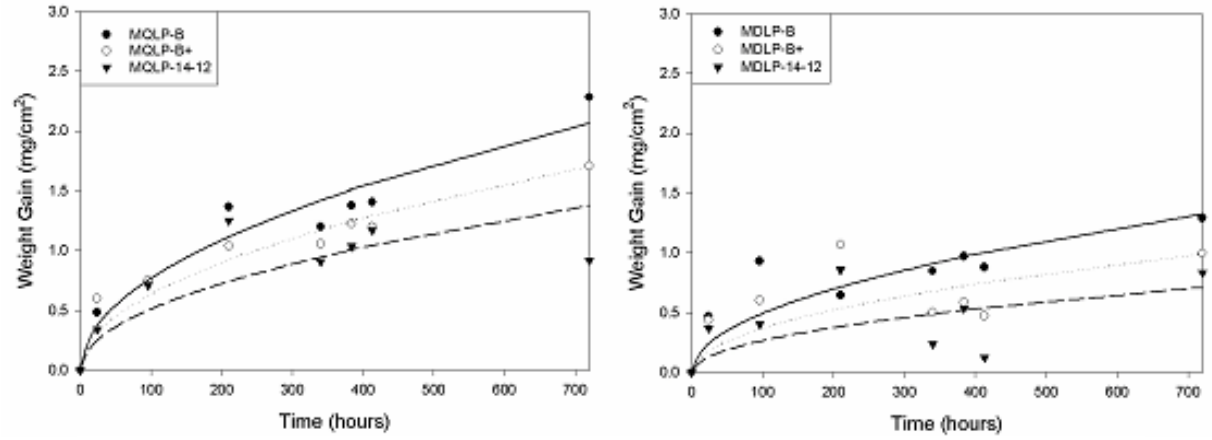

Figure 9: Weight gain due to oxidation in 85°C/85% RH chamber test for controls MQP™-B+ and MQP™-14-12 (left) and microdispersion-coated MQP™-B+ and MQP™-14-12 (right).

4. Effects of powder morphology

The near net shape production of bonded magnets is one of the great advantages that isotropic bonded magnets have over their fully dense anisotropic alternatives, and injection molding is the most economical means for high volume production. One of the most important characteristics for injection molding is the rheology of polymer melt (mixture of molten polymer and MQP™ powder). Figure 10 is a schematic of injection molding processibility with respect to the volume fraction of magnetic powder in the polymer melt. As can be seen, the processibility decreases with increasing volume fraction of magnetic powder, which in turn limits the net B_r and $(BH)_{max}$ in the associated bonded magnets. One technique used to improve the processibility and maintain a high volume fraction of magnetic powder is the use of powder with a more spherical or cubic morphology.

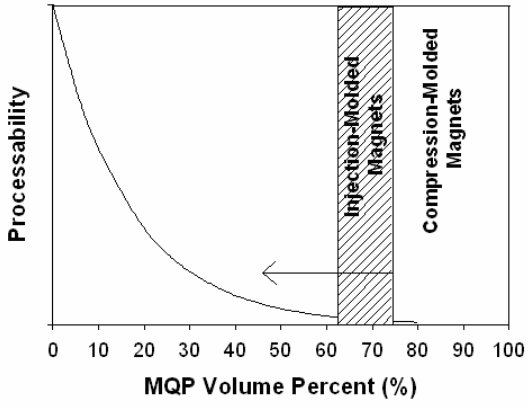

Figure 10: Schematic of injection molding processibility with respect to the volume fraction of magnet powders in the polymer melt.

4.1 Improvement in the rheological behavior of polymer melt

Figure 11 compares the relationship between apparent viscosity with respect to applied shear stress for five different types of polymer melt, using a fixed volume fraction (62 vol%) of magnet powder and using polyamide 11 (Nylon-11) as the polymer binder; these results simulate the typical injection molding process. The polymer melt that exhibits the most favorable rheological behavior (low apparent viscosity) contains atomized R-Fe-B powder (MQP™-S-11-9) having a spherical morphology, while the polymer melt that offers the most resistance to being molded contains the melt-spun flake powder (e.g. MQP™-B). The three curves between these two represent the processing behavior of mixed flake/spherical powder blends (MQP™-B:MQP™-S-11-9 of 3:1, 1:1 and 1:3). Since lower apparent viscosity at a given applied shear stress is usually more desirable for

injection molding, this suggests that atomized powder with spherical morphology is the most suitable in terms of processibility. However, atomized powder is quenched at lower rates (typically 10^5/sec) than conventional melt spun flake material (~10^6/sec), so alloying additions must be combined with the $R_2Fe_{14}B$ stoichiometric composition for atomized powder to avoid coarse under-quenched microstructures. Hence, atomized powders tend to give slightly lower B_r values in comparison to melt spun materials of the same composition, but a dilute addition of atomized powder into conventional melt-spun powder provides a compromise between good magnetic properties and favorable rheology of the polymer melt.

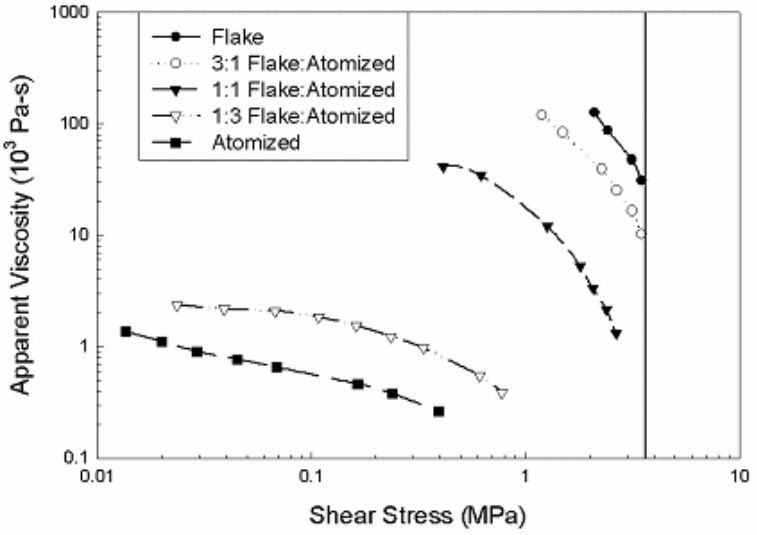

Figure 11: Comparison of the relationship between apparent viscosity and applied shear stress for five different types of polymer melt with a fixed volume fraction (62 vol%) of magnetic powder and using polyamide 11 (Nylon-11) as the polymer binder, processed at 280°C.

4.2 Melt spun powders of low aspect ratio

The processing advantages to the polymer melt of spherical powder may be realized also with flake materials by reducing their aspect ratio (the width to thickness ratio). By milling a near stoichiometric melt-spun composition to a more nearly cubic morphology, both high remanence and low apparent viscosity of the polymer melt can be achieved.

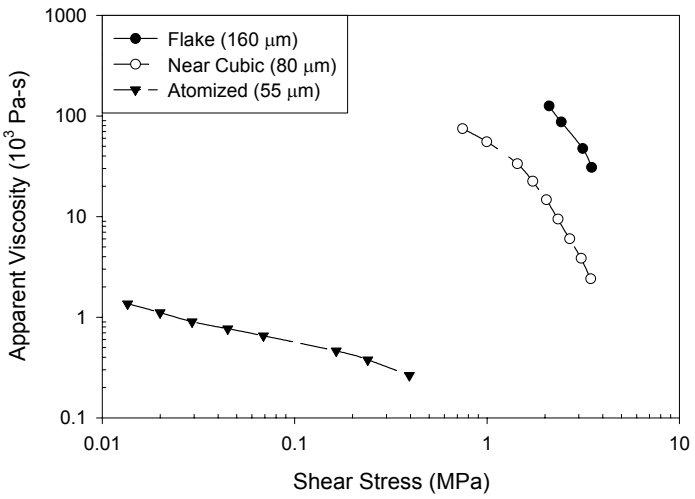

Figure 12: Comparison of the relationship between apparent viscosity and shear stress of the polymer melt prepared from flake materials of low aspect ratio with that of conventional flake materials and atomized powder at 62 vol% of magnet powder using polyamide 12 as the polymer binder.

Figure 12 compares the apparent viscosity for three polymer melts with different powder morphologies. The mean particle size of these magnetic powders (determined by conventional sieve analysis) was 55μm for the spherical atomized powder, 80μm for the near-cubic melt-spun flake powder, and 160μm for the conventional commercial melt-spun flake material of high aspect ratio. Section 4.1 demonstrated the advantages of atomized powders for improved processibility, and it is now evident that the near cubic powders generally show similar processing benefits. An order of magnitude drop in apparent viscosity (compared to conventional flake powder) is observed when the near-cubic powders are used, and this represents a significant improvement in

injection molding performance. A decrease in the apparent viscosity implies that lower shear stresses can be applied and that a higher volume fraction of magnetic powder can be utilized within the same injection molding limits, with a consequent gain in B_r for the bonded magnet.

4.3 Importance of loop squareness

It was mentioned in Section 1, with particular regard to the application of the nanocomposite powder with very high B_r, that good squareness in the demagnetization curve is very important. To illustrate this, a finite element (FEA) model of powder in a bonded magnet has been constructed as shown in Figure 13. The powder is assumed to be spherical to simplify the calculation, but the results would be similar for melt spun powders of low aspect ratio as described above. The particles are arranged according to their actual volumetric loading and are assigned their true demagnetization characteristics. Then the FEA calculates the magnetic field in the magnet as a whole, thus allowing for self-demagnetization and deducing the actual B_r that the magnet will exhibit. The ratio of this to the powder's B_r (if not unity) indicates that there is an "apparent" volumetric loading, different from the actual.

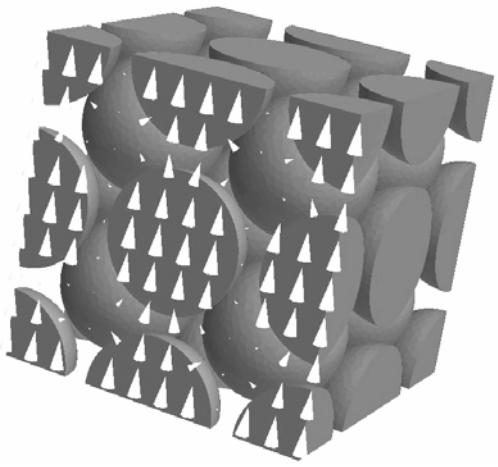

Figure 13: Finite element analysis model of powder particles in a typical volumetric loading, showing computed internal magnetic field vectors.

Table 2 compares milled flake powder having the magnetic properties of MQP™-16-7 with a pseudo-spherical powder having a comparable B_r but much inferior H_{ci}. The lower H_{ci} is accompanied by a demagnetization curve which has poorer loop squareness, so it is seen that even though we allow the "spherical" powder to have 5% greater loading (as would typically be applied to such morphology), the bulk magnet actually exhibits a lower B_r than the higher H_{ci} flake powder, and a lower "apparent" volumetric loading.

Table 2: Results of FEA analysis giving calculated B_r and "apparent" loading factor in bulk magnet made from powders.

Powder Type	Powder H_{ci}	Powder B_r	Magnet B_r	Actual volumetric loading	"Apparent" volumetric loading
MQP™-16-7 flake powder:	557kA/m	980mT	580mT	61%	58.7%
High B_r "spherical" powder:	350kA/m	960mT	535mT	66%	55.7%

Conclusions

New applications continue to demand improved properties from bonded magnets which employ melt-spun $R_2Fe_{14}B$-type powders. Market trends for the products in which these materials are used, such as greater miniaturization and higher operating temperatures, have led to the recent introduction of improved powder grades.

A $R_2Fe_{14}B/\alpha$-Fe nanocomposite powder (Magnequench grade MQP™-16-7) achieves a B_r of 980mT, which is the highest available in a commercial $R_2Fe_{14}B$ rapid solidified powder. A low flux aging loss powder (Magnequench grade MQP™-14-12) has been found to be suitable for operating at temperatures as high as 180°C with low flux aging loss. A microdispersion coating process was found to reduce this loss by approximately 30% at 180°C in MQP™-14-12, and this improvement in

flux aging performance now allows MQP™-14-12 based magnets to be used up to 220°C for high temperature applications.

The apparent viscosity of a polymer melt can be adjusted by blending conventional flake powder with spherical atomized rapidly solidified powder in predetermined ratios, but reduction in the aspect ratio of flake powder was also found to improve the apparent viscosity by an order of magnitude at the same shear stress, when compared to the conventional flake powder. This enables better injection molding characteristics to be combined with the high B_r provided by near stoichiometric melt-spun powder compositions.

References

[1] E.F. Kneller and R. Hawig, *IEEE Trans. Magn***. 27** (1991) 3588.
[2] A. Manaf, M. Leonowicz, H.A. Davies, R.A. Buckley, *J. App. Phys.***, 70** (1991) 6366.
[3] W.C. Chang, D.M. Hsing, B.M. Ma, and C.O. Bounds, IEEE Trans. on Magn., **32**, (1996) 4425..
[4] Z. Chen, Y.Q. Wu, M.J. Kramer, B. Smith, B.M. Ma and M.Q. Huang, *J. Magn. Magn. Mater*., **268**, 105 (2004).